On the basis of these preliminary results, we conclude that the peak is due to a free radical intermediate formed by the addition of AIBN to MMA or by AIBN in MMA. This free radical is probably stabilized through conjugation with either the cyano group or the ester group. The fact that we were able to obtain a good signal from a reaction intermediate which presumably is very low in concentration and relatively short-lived suggests that there must be a significant enhancement of the Raman band by resonance. Since our excitation wavelength was 488.0 nm, a conjugated system is needed. We plan to check whether the signal is due to resonance Raman scattering or not in the near future.

IV. Conclusions

We have successfully demonstrated the use of Raman and FTIR spectroscopy for monitoring polymerization of styrene and MMA in real time. Contrary to the previously recommended procedure, monitoring only the integrated peak area of the double-bond peak at 1631 cm^{-1} for Raman and 1643 cm^{-1} for IR introduces less total error compared to using an internal reference band. The activation energies and the initial rates of polymerization determined from spectroscopic data compare very favorably with the classical data for styrene polymerization.

We see a lower rate of polymerization in our IR cell than the Raman cell. This can be due to the fact that the IR cell has a high surface-to-volume ratio compared to the Raman cell. Another possibility is the presence of oxygen and a lot of metallic surface in the IR cell. We observe some indications of the Trommsdorf effect with thermal polymerization of styrene but it is much more readily observable for MMA polymerization.

This investigation also shows the value of simultaneous detection of a wide frequency range of the Raman spectrum. As a result of the fact that we detected all the signal in a 1300-cm^{-1} range, we were able to observe the presence of a reactive intermediate, probably a stabilized free radical, when the polymerization rate increases in the initiated MMA system. We are planning on continuing our research in this area in order to find out more about the reactive intermediates.

Acknowledgment. We gratefully acknowledge the support of this research by the Polymers Program of the NSF, Grant DMR-8100130. We also thank Ms. K. J. Lee for taking some of the data and to the reviewers of the first submitted version of this paper for their valuable comments.

Registry No. Styrene, 100-42-5; methyl methacrylate, 80-62-6.

References and Notes

(1) Patterson, G. D.; Stevens, J. R.; Alms, G. R.; Lindsey, C. P. *Macromolecules* **1979**, *12*, 658.
(2) Chu, B.; Fytas, G. *Macromolecules* **1982**, *15*, 561.
(3) Coakley, R. W.; Mitchell, R. S.; Hunt, J. L.; Stevens, J. R. *J. Macromol. Sci., Phys.* **1976**, *12*, 511.
(4) Alms, G. R.; Patterson, G. D.; Stevens, J. R. *J. Chem. Phys.* **1979**, *70*, 2145.
(5) Jeffrey, K. R.; Stevens, J. R. *J. Chem. Phys.* **1979**, *71*, 2331.
(6) Chu, B.; Fytas, G.; Zalczer, G. *Macromolecules* **1981**, *14*, 395.
(7) Sears, W. M.; Hunt, J. L.; Stevens, J. R. *J. Chem. Phys.* **1981**, *75*, 1599.
(8) Tulig, T. J.; Tirrell, M. *Macromolecules* **1982**, *15*, 459.
(9) Boundy, R. H.; Boyer, R. F., Eds. "Styrene, Its Polymers, Copolymers, and Derivatives"; Hofner Publishing Co.: New York, 1952.
(10) Allen, P. E. M.; Patrick, C. R., Eds. "Kinetics and Mechanisms of Polymerization Reactions"; Wiley: New York, 1974.

Hydrodynamic Thickness of Adsorbed Polymer Layers

Martinus A. Cohen Stuart* and Frank H. W. H. Waajen

Laboratory for Physical and Colloid Chemistry, 6703 BC Wageningen, The Netherlands

Terence Cosgrove,* Brian Vincent, and Trevor L. Crowley

University of Bristol, Cantock's Close, Bristol BS8 1TS, United Kingdom.
Received July 13, 1983

ABSTRACT: Hydrodynamic thicknesses of adsorbed polymer layers have been calculated on the basis of a porous layer model using segment density profiles calculated with the Scheutjens–Fleer adsorption theory. Comparisons of the molecular weight and adsorbed amount dependence of the hydrodynamic thickness are made with experimental data obtained by photon correlation spectroscopy on a system of polystyrene latex particles dispersed in aqueous poly(ethylene oxide) solutions. It is confirmed that tails play a very important role in the screening of the adsorbed layer from the flow field.

Introduction

An early study of Öhrn[1] was the first to appreciate the considerable effect of an adsorbed polymer on liquid flow through a capillary. More recently, this effect has been exploited by a number of research groups in order to characterize adsorbed layers by means of a "hydrodynamic" thickness. The experimental techniques used are in most cases based on the reduction of flux of solvent when a polymer is adsorbed on the wall of a suitable flow channel. Various materials have been used, for example, sintered glass disks,[2] porous membranes, single glass capillaries,[3] or capillary arrays. An alternative approach is to measure the increase in radius of a colloidal particle upon adsorption by means of its sedimentation[4] or diffusion[4,5] coefficient.

Because of difficulties in the interpretation of the hydrodynamic thickness, the interpretation of experimental data has been purely qualitative. However, in a recent paper Varoqui and Degardin[6] have given an analytical solution of an appropiate hydrodynamic equation for the case of a capillary with an adsorbed layer. Their approach is instructive as it gives an explanation for the experimental observation that the hydrodynamic thickness is often much larger than the layer thickness determined

0024-9297/84/2217-1825$01.50/0

optically by ellipsometry[7] and by neutron scattering.[8] In this paper we extend the approach of ref 6 to overcome two of its limitations.

First, we use segment density profiles obtained from the Scheutjens and Fleer theory.[9] Unlike the Hoeve[10] theory used in ref 6, the Scheutjens–Fleer theory takes proper account of the density distribution associated with tails. This is likely to be most important in determining the solvent flow at the periphery of the adsorbed layer.

Second we introduce friction factors derived experimentally from sedimentation experiments following the papers by Mijnlieff et al.[11,12] This overcomes a serious limitation of Dejardin's model which uses the Stokes equation to find the friction exerted by segments, which does not take into account the effects of hydrodynamic interactions. Another disadvantage of the Stokes equation is that the limiting behavior at high segment density is incorrect.

In the following sections the details of the theory are outlined and comparisons are made with experimental layer thicknesses obtained by photon correlation spectroscopy (PCS).

Theoretical Calculations

Procedure. The starting point for this analysis is to use the multilayer adsorption theory of Scheutjens and Fleer.[9] In this theory, the solution between a pair of plane adsorbent/solution interfaces is divided into layers (1, ..., i, ..., M) of lattice sites parallel to the interfaces. Each lattice site is occupied by either a polymer segment or by solvent and, hence, each layer is characterized by one volume fraction ϕ_i of segments. The thickness of each layer, a, is taken to be equal to the cross section of the polymer chain.

We now consider laminar flow between the two walls, covered with adsorbed polymer, and write a Debye–Brinkman equation for each layer i

$$\eta_0 \frac{d^2 v_i}{dx^2} - \eta_0 \frac{v_i}{k_i^2} = -\text{grad } P \tag{1}$$

Here, v_i is the liquid velocity parallel to the walls, x is the distance normal to the walls, η_0 is the viscosity of the solvent, and P is the pressure. The constant k_i is a friction factor, depending only on ϕ_i. For convenience, eq 1 is rewritten in dimensionless form

$$\frac{d^2 u_i}{dy^2} - \frac{u_i}{q_i^2} + 1 = 0 \tag{2}$$

where the following substitutions have been made:

$$y = x/a \tag{3}$$

$$u_i = (v_i \eta_0)/(a^2 \text{ grad } P) \tag{4}$$

$$q_i = k_i/a \tag{5}$$

As a consequence the calculated hydrodynamic thickness is in units of a. Note that the dimensionless distance y for each layer varies from 0 to 1.

The general solution of eq 2 can be written as

$$u_i = C_i^s \sinh (y/q_i) + C_i^c \cosh (y/q_i) + q_i^2 \tag{6}$$

$$du_i/dy = \frac{1}{q_i}\{C_i^s \cosh (y/q_i) + C_i^c \sinh (y/q_i)\} \tag{7}$$

At the boundaries of layer i ($y = 0$ and $y = 1$, respectively), the following boundary conditions connect layer i to layer $i + 1$:

$$u_{i+1}(0) = u_i(1) \tag{8}$$

$$(du_{i+1}/dy)_{y=0} = (du_i/dy)_{y=1} \tag{9}$$

implying a continuous velocity and a continuous velocity gradient, respectively. The constants C_i^s and C_i^c are given by

$$C_i^s = q_i(du_i/dy)_{y=0} \tag{10}$$

$$C_i^c = u_i(0) - q_i^2 \tag{11}$$

At the adsorbent surfaces, the velocity is necessarily zero

$$u_i(0) = u_M(1) = 0 \tag{12}$$

Halfway between the plates (at $i = M/2$) the velocity gradient must vanish

$$(du_{M/2}/dy) = B = 0 \tag{13}$$

In general, the distance between the plates will be much larger than the hydrodynamic thickness δ_H ($\delta_H/M \ll 1$), which ensures that the opposing adsorbed layers do not interact; δ_H is then independent of the dimensions of the flow channel. The result is also applicable for other geometries (e.g., spheres and cylindrical capillaries) provided that the radius of curvature is large compared to the thickness of the adsorbed layer.

Segments of nonadsorbing chains are not taken into account in this calculation of k_i. Hence, there is a region between the plates where the friction term in eq 1 vanishes. In this region, eq 6 and 7, for the boundary $y = 1$, reduce to

$$u_i(1) = u_i(0) + (du_i/dy)_{y=0} - \tfrac{1}{2} \tag{14}$$

and

$$(du_i/dy)_{y=1} = (du_i/dy)_{y=0} - 1 \tag{15}$$

We now calculate the complete velocity profile by means of a simple two-step iteration. Starting at the wall with $u_1(0) = 0$ (eq 12) and an arbitrary gradient $(du_1/dy)_{y=0} = A$, we calculate the velocity and velocity gradient at the boundary between layer 1 and layer 2 (eq 6, 7, 10, and 11). According to the boundary conditions (8) and (9) we then have the velocity and velocity gradient at $y = 0$ in layer 2. Proceeding in this way from layer to layer (replacing eq 6 and 7 by eq 14 and 15, respectively, for those layers where $\phi_i = 0$) we eventually find the velocity gradient B at $i = M/2$. A must then be adjusted such that condition (13) is fulfilled. It can be shown that B varies linearly with A and hence, the velocity profile is calculated again with a new value for A. The resulting value for B is used to perform a linear extrapolation of A toward $B = 0$. Finally, the total flux J is calculated as

$$J = \sum_i^M \int_0^1 u_i \, dy \tag{16}$$

This flux is smaller than the flux J_0 between plates with no adsorbed polymer at a separation M. The same flux, however, can be attained by moving the bare plates together by a distance $2\delta_H$. Therefore we define the hydrodynamic thickness δ_H by means of the relation

$$J = 2 \int_{\delta_H}^{M/2} u' \, dx \tag{17}$$

where $u'(x)$ is the velocity profile between the bare plates at a distance $M - 2\delta_H$.

In practice, the walls of the flow channel are fixed and the experimental layer thickness is obtained from the flux ratio J/J_0:

$$(M - \delta_H)^3/M^3 = J/J_0 \quad \text{for parallel plates} \tag{18a}$$

$$(M - \delta_H)^4/M^4 = J/J_0 \quad \text{for cylindrical capillairies} \tag{18b}$$

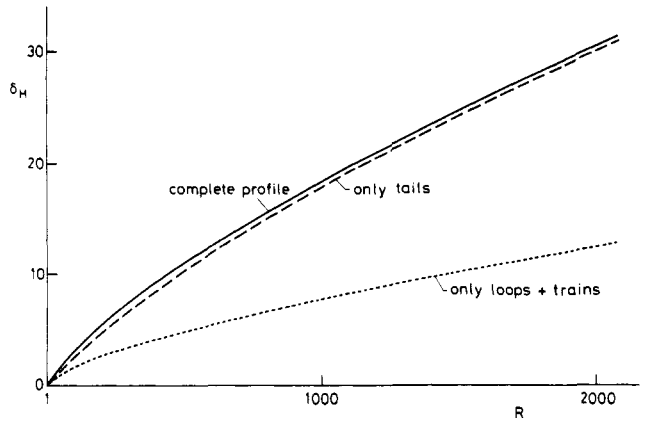

Figure 1. Hydrodynamic layer thickness δ_H as a function of chain length R. Segmental adsorption energy $\chi_s = 1$, Θ solvent ($\chi = 0.5$), equilibrium volume fraction of polymer $\phi_* = 10^{-3}$, hydrodynamic constant $c/a^2 = C_H = 1$. Full curve, complete segment density profile; dashed curve, only tails; dotted curve, only loops and trains.

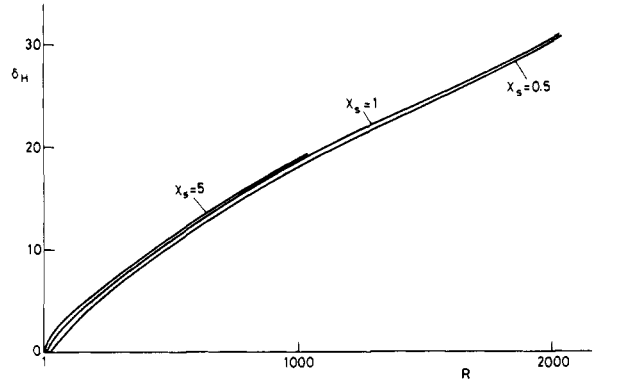

Figure 2. δ_H as a function of chain length R for various adsorption energies. Same parameters as a Figure 1; the values of the segmental adsorption energy for each curve are indicated in the figure.

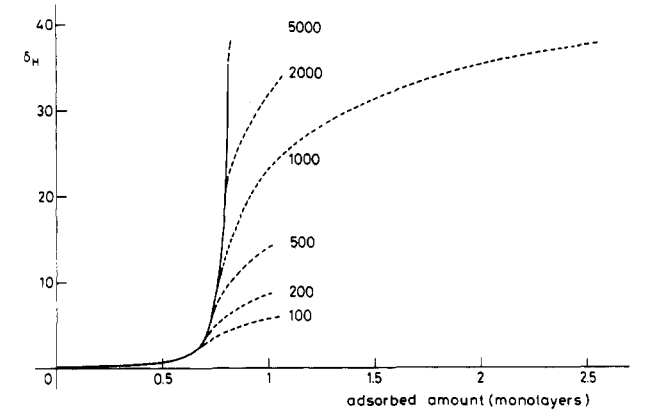

Figure 3. δ_H as a function of adsorbed amount Γ for various chain lengths. The curves coincide at low bulk concentration (full curve) but diverge as the bulk concentration increases (dotted curves). The chain length of each curve is indicated; $\chi_s = 1$, $C_H = 1$, athermal solvent ($\chi = 0$). Four poor solvents ($\chi = 0.5$) the dependence is qualitatively similar but less steep.

A computer program was developed. Copies (in SIMULA or FORTRAN) will be made available on request.

Theoretical Predictions

Values of δ_H were calculated for numerous cases using segment density profiles generated by the theory of Scheutjens and Fleer. For the permeability in layer i, denoted by k_i, a set of experimental values is required for each particular case. This set can in principle be determined by Mijnlieff's procedure.[11,12] However, for the sake of illustration we attempted to replace the empirical relation $k(\phi)$ by a simple function with as few adjustable parameters as possible. Available data[11,13] suggest the form

$$k_i^2 = c\frac{1-\phi_i}{\phi_i} \tag{19}$$

where c is a constant for a given polymer. Note that this equation has the correct limiting behavior, both at $\phi_i = 0$ and at $\phi_i = 1$.

The dependency of the hydrodynamic layer thickness on various adsorption parameters is summarized in Figures 1–6. For most figures we chose $c/a^2 = C_H = 1$ as the value

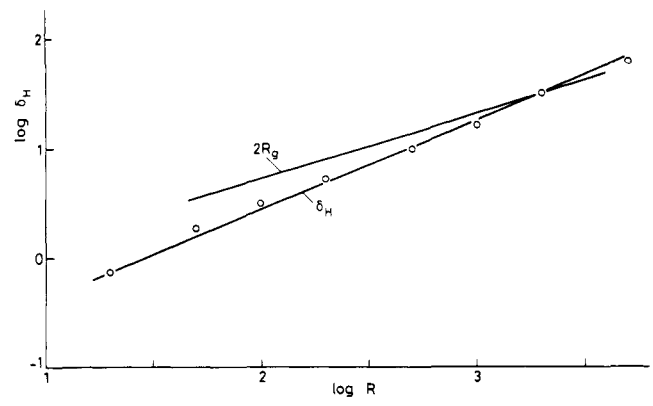

Figure 4. log (δ_H) as a function of log (R). $\chi_s = 1$, $\chi = 0.45$, $C_H = 0.5$, equilibrium concentration $\phi_* = 10^{-4}$. The diameter of free coils, given as twice the radius of gyration R_g, is also shown. R_g was calculated as $R_g = 0.17R^{0.6}$.

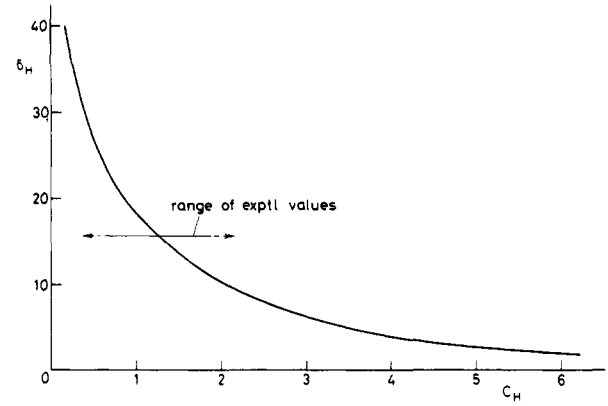

Figure 5. δ_H as a function of the hydrodynamic constant C_H ($=c/a^2$). $\chi_s = 1$, $\chi = 0.5$, $\phi_* = 10^{-3}$, $R = 1000$. Experimental values of C_H will probably occur in the range indicated in the figure.

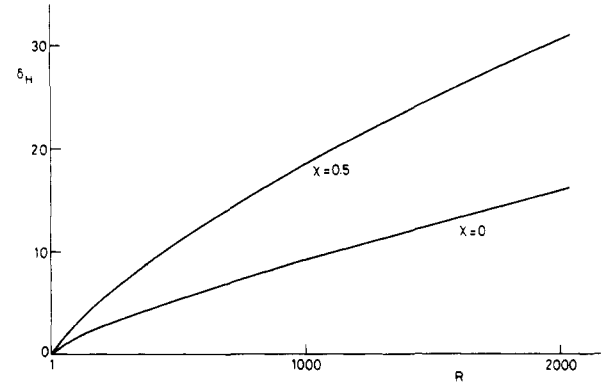

Figure 6. Dependence of δ_H on chain length R for an athermal solvent ($\chi = 0$) and for a Θ solvent ($\chi = 0.5$). $\chi_s = 1$, $C_H = 1$, $\phi_* = 10^{-3}$. The value of the χ-parameter for each curve is indicated in the figure.

for the hydrodynamic constant. This choice is in accordance with results of Mijnlieff,[12] who found that c is of the order of 10^{-18} m^2, and with an estimate of the thickness of an elementary layer of about 1 nm. In Figure 5 we give also the dependence of δ_H on C_H. We shall discuss the dependence of other results on this parameter.

In Figure 1 we present δ_H as a function of the chain length R. The full curve gives the hydrodynamic layer thickness for the complete segment density profile. The dependency is approximately linear, at least for large R. The dashed curve was obtained for a segment profile from which trains and loops were omitted, i.e., which is equivalent to assuming that these segments had zero friction. In this case, δ_H is only slightly reduced with respect to the complete profile. For long chains the difference is not more than a few percent. This is an interesting result, showing that the hydrodynamic layer thickness is almost completely determined by the tails; trains and loops are effectively screened from the liquid flow. A completely different result is obtained if the screening by tails is removed, i.e., if only loops and trains are assigned a nonzero friction. The thickness obtained in that way is smaller by a factor of about 4 as compared to the full profile (see Figure 1, dotted curve). The profile assumed by Varoqui et al.[6] was based on Hoeve's theory, where tails are supposed not to contribute.[10] This result shows that neglecting the tail segments substantially underestimates the hydrodynamic thickness.

Further evidence of the importance of tails is obtained from Figure 2, where we plot δ_H as a function of the segmental adsorption energy χ_s. A high χ_s means strong adsorption, high adsorbed amounts, and a high segment density in the layers close to the adsorbent surface.[9] However, the adsorbed amount in tails and the tail length are hardly affected. From Figure 2 we see that δ_H depends hardly on χ_s. Hence, although loop and train contributions change dramatically, there is no effect on δ_H because of the strong hydrodynamic screening by the tails.

In Figure 3 we give the dependence of δ_H on the adsorbed amount, Γ. A family of S-shaped curves is found, one for each chain length. These curves all coincide for adsorbed amounts corresponding to low bulk concentrations, whereas at higher bulk concentration the curves level off at a plateau characteristic for the chain length. Scheutjens and Fleer, calculating values for the root-mean-square layer thickness t as a function of Γ, found a similar set of curves. We may conclude that for δ_H it is irrelevant whether Γ is the result of the adsorption of short chains or of long chains, provided the solution is dilute. At low Γ layer thicknesses are small because the surface is not saturated and the polymer molecules adsorb in a flat conformation with hardly any tails. When the segment density close to the surface approaches saturation, loops and tails develop, and due to the latter, we observe a strong increase in δ_H, which levels off as the bulk concentration approaches the overlap concentration. As far as we can infer, there is no limit to the maximum obtainable δ_H as a function of chain length.

In Figure 4 we compare δ_H with the cross section of a free coil in solution, as measured by $2R_g$; both δ_H and $2R_g$ are plotted logarithmically as a function of log R. For our (theoretical) case, R_g is assumed to follow the lower law for self-avoiding walks, i.e., $CR^{0.6}$, where C is a constant characteristic for a given polymer. Four our plot, we chose $C = 0.17$. In view of experimental results to be discussed below, we chose for this particular plot $C_H = 0.5$, although this only affects the quantitative aspects. As can be seen from Figure 4, δ_H increases more strongly than R_g. The plot gives a slope of 0.8 ± 0.03. For short chains, therefore, δ_H may be much smaller than the diameter of a free coil. As tails develop, δ_H increases rapidly and may eventually become larger than $2R_g$.

Table I
Molecular Weight, Hydrodynamic Layer Thickness (δ_H), Adsorbed Amount (Γ), and Radius of Gyration (R_g) for Poly(ethylene oxide) (PEO) Samples Used in This Work

$M_w \times 10^{-3}$	M_w/M_n	δ_H, nm	Γ, mg m^{-2}	R_g, nm
25	1.14	58 ± 1.5	0.56 ± 0.05	6.5
40	1.03	12.0 ± 3.0	0.68 ± 0.05	10.0
73	1.02	17.3 ± 5.0	0.89 ± 0.05	13.5
150	1.04	29 ± 3.0	0.99 ± 0.05	19.1
280	1.05	53 ± 3.0	1.21 ± 0.05	29.4
660	1.10	95 ± 10	1.42 ± 0.05	45.5
1290	1.12	160 ± 10	1.57[a]	63.6

[a] Estimated by extrapolation (see Figure 7).

The results discussed so far do not change qualitatively when the permeability constant C_H for the polymer is changed. However, quantitative changes do of course occur, as shown in Figure 5. At very low C_H, the layer thickness increases strongly, because the polymer becomes virtually impermeable to solvent. At high C_H, δ_H becomes very low because the friction exerted by segments practically vanishes. In most cases we expect C_H to vary between narrow limits, as indicated in the figure.

The effect of solvent quality as expressed in the FH parameter χ is shown in Figure 6. For good solvents ($\chi = 0$) lower layer thicknesses are found than for Θ solvents ($\chi = 0.5$) *assuming that C_H is the same in both solvents.* However, Mijnlieff[12] observed that for Θ solvents the permeability was always higher than for good solvents, probably as a result of a tendency of the segments to form clusters, thereby reducing the hydrodynamic friction. In calculating δ_H for different χ values, the adsorbed amount has not been held constant and thus the expected effect of the adsorbed chains expanding in a good solvent environment is overridden by the decrease in the adsorbed amount.

Experimental Section

Photon correlation spectroscopy (PCS) was used to determine the hydrodynamic thickness of narrow-distribution poly(ethylene oxide) (PEO) over the molecular weight range 2.5×10^4 to 1.29×10^6. Details of the samples, which were obtained from Toya Soda Co. (Japan) are given in Table I. The polystyrene latex sample was prepared by a surfactant-free method, using potassium persulfate as the initiator. The resulting particles had a diameter of 240 ± 4 nm from PCS and 237 ± 5 nm from electron microscopy. The PCS equipment consisted of a coherent, mode-stabilized krypton laser operating at 647 nm and a Malvern Instruments spectrometer and multibit correlator. The resulting time correlation functions were analyzed by a nonlinear least-squares program run on a PDP-11 computer. Adsorption isotherms for the samples were obtained by using an interferometer to analyze the equilibrium concentration of PEO in the supernatant. For the PCS experiments, samples were made up by first diluting the stock latex to a solids content of 0.02% and subsequently adding the required concentration of polymer to obtain an equilibrium concentration of 200 mg/L.

Discussion

In Figure 7 we present data for the adsorbed amount as a function of molecular weight. A corresponding theoretical plot, based on the Scheutjens–Fleer theory choosing $\chi = 0.45$ (from experimental data) and $\chi_s = 1$, is shown in Figure 8. Both plots are linear and have slopes of 0.6 mg m^{-2} and 0.6 monolayers, respectively. This suggests that for PEO an equivalent monolayer corresponds to 1 mg m,$^{-2}$ which is reasonable as compared to

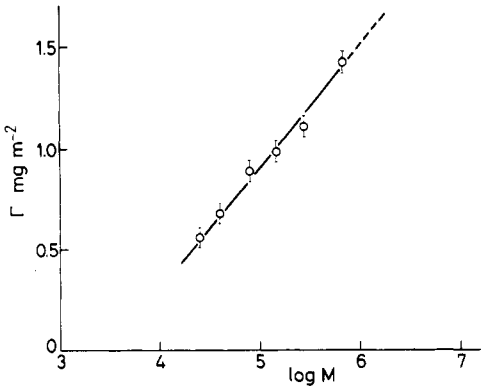

Figure 7. Adsorbed amount Γ of poly(ethylene oxide) (PEO) from water on polystyrene (PS) latex as a function of log (M), where M is the molar mass in g mol^{-1}. The curve has been extrapolated to obtain a value of Γ at $M = 1.29 \times 10^6$.

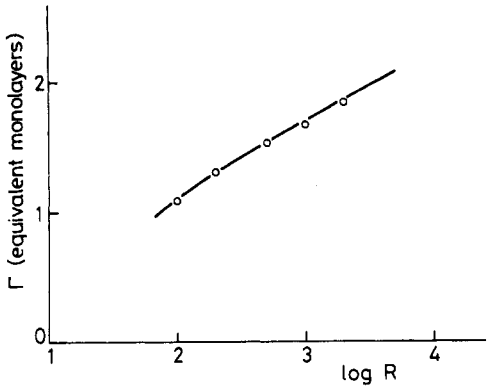

Figure 8. Adsorbed amount Γ according to the Scheutjens–Fleer theory[9] as a function of log (chain length). $\chi_s = 1$, $\chi = 0.45$, $\phi_* = 10^{-4}$.

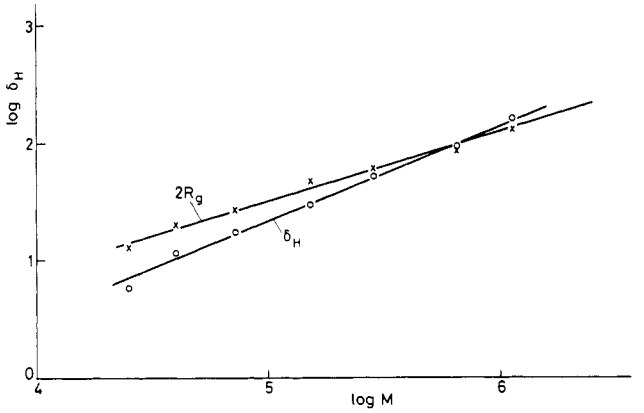

Figure 9. log (δ_H) for PEO adsorbed from water on PS latex as a function of log (M) (circles). For comparison, $2R_g$ (from light scattering) is also shown (crosses).

a value of 0.4 mg m^{-2} estimated with the known density and monomer size of PEO.

In Figure 9 we plot the hydrodynamic thickness logarithmically as a function of log (molecular weight). Essentially identical results have been reported by Kato et al.[5] Comparison can be made with the corresponding theoretical plot given in Figure 4, using $\chi = 0.45$ and $\chi_s = 1$. The permeability constant for PEO (eq 19) has been determined from sedimentation experiments as 0.5 nm^2.[14] The theoretical plot (Figure 4) was obtained by using 1 nm for the elementary layer thickness and a value of c of 0.5 nm^2. For the sake of comparison, we also included experimental values of $2R_g$ in Figure 9.

The agreement between Figures 4 and 9 is very satisfactory. In both plots we observe that for short chains δ_H is below the diameter of the free coil, but due to its stronger dependence on R, δ_H eventually becomes larger than $2R_g$. The slope of the experimental plot is 0.8 ± 0.05, in excellent agreement with the theoretical value of 0.8 ± 0.03. A crossover between $2R_g$ and δ_H is observed at a molecular weight of about 7×10^5, but as we do not know the numerical constant for the theoretical value of R_g, it is not possible to compare with a theoretically predicted crossover.

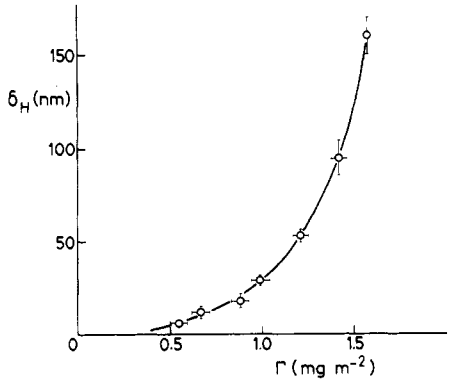

Figure 10. Hydrodynamic layer thickness δ_H as a function of adsorbed amount Γ for PEO adsorbed from water on PS latex.

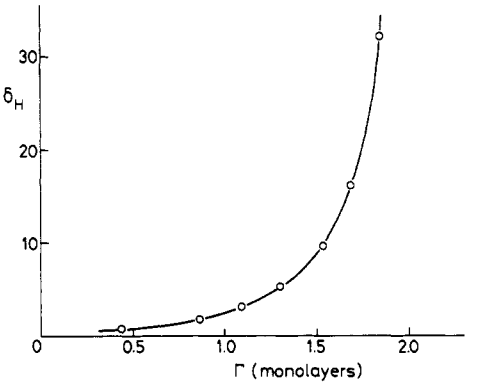

Figure 11. Theoretical value of δ_H as a function of adsorbed amount according to the Scheutjens–Fleer theory.[9] $\chi_s = 1$, $\chi = 0.45$, $\phi_* = 10^{-4}$, $C_H = 0.5$.

Finally, in Figure 10, we plot experimental results for δ_H as a function of adsorbed amount; the corresponding theoretical plot is shown in Figure 11. Again we observe similar trends in both graphs, namely, a very low thickness at low coverage, followed by a steep increase in δ_H as the adsorbed amount exceeds a certain thereshold. We conclude that the qualitative agreement between theory and experiment is very good indeed.

For a quantitative comparison we must introduce at least two scaling factors, namely, one relating the number of segments to the molecular weight (this is not necessarily the monomer weight) and one relating the number of layers calculated by theory to the experimental thickness. Both scaling factors depend in some way on the structural properties of the particular polymer used (e.g., size of the monomer or flexibility of the chain) and are therefore not independent.

One approach to this scaling problem is to utilize the dependence of hydrodynamic thickness on molecular weight, because of the good agreement between the scaling exponents. For example, if we choose 2 monomers per theoretical segment and 1.1 nm per elementary layer, the theoretical and experimental results can be exactly superimposed. Such a choice can be rationalized on the basis of a comparison of characteristic ratios of the real, physical chain and the theoretical lattice chain.

The main conclusion from this work is that the porous layer model, combined with the Scheutjens–Fleer adsorption theory is able to predict the variation of hydrodynamic layer thickness of adsorbed polymer layers with coverage and with molecular weight quite well. The dominant contribution to this thickness comes from long tails, which extend far into the solution.

Acknowledgment. We acknowledge NATO for providing funds for the continued collaboration between Bristol and Wageningen. SERC is acknowledged for providing money for equipment (PCS) and for a joint ICI/SERC postdoctoral fellowship (T.L.C.). J. Bishop and P. Collier are thanked for providing the PCS data, and G. Fleer and J. Scheutjens for stimulating discussions.

References and Notes

(1) Öhrn, O. E. *Ark. Kemi* **1958**, *12*, 397.
(2) Rowland, F. W.; Eirich, F. R. *J. Polym. Sci., Part A-1* **1966**, *4*, 2401.
(3) Priel, Z.; Silberberg, A. *J. Polym. Sci., Polym. Phys. Ed.* **1979**, *16*, 1917.
(4) Garvey, M. J.; Tadros, Th. F.; Vincent, B. *J. Colloid Interface Sci.* **1976**, *55*, 440.
(5) Kato, T.; Nakamura, K.; Kawaguchi, M.; Takahashi, A. *Polym. J.* **1981**, *13*, 1037.
(6) Varoqui, R.; Dejardin, P. *J. Chem. Phys.* **1977**, *66*, 4395.
(7) Takahashi, A.; Kawaguchi, M.; Kayashi, K.; Kato, T. *ACS Symp. Ser.* **1984**, *No. 240*, 39.
(8) Barnett, K. G.; Cosgrove, T.; Vincent, B.; Burgess, A. N.; Crowley, T. L.; King, T.; Turner, J. D.; Tadros, Th. F. *Polymer* **1981**, *22*, 283.
(9) Scheutjens, J. M. H. M.; Fleer, G. J. *J. Phys. Chem.* **1979**, *83*, 1619; **1980**, *84*, 178.
(10) Hoeve, C. A. J. *J. Polym. Sci., Part C* **1970**, *30*, 361; **1971**, *34*, 1.
(11) Mijnlieff, P. F.; Jaspers, W. J. *Trans Faraday Soc.* **1971**, 67, 1837.
(12) Mijnlieff, P. F.; Wiegel, F. W. *J. Polym. Sci., Polym. Phys. Ed.* **1978**, *16*, 245.
(13) Vidakovic, P.; Allain, C.; Rondelez, F. *Macromolecules* **1982**, *15*, 1571.
(14) Cosgrove , T.; Cohen Stuart, M. A.; Crowley, T. L.; Vincent, B. *ACS Symp. Ser.* **1984**, *No. 240*, 53.

Properties of Partially Cured Networks. 1. Curing Kinetics of a Model Network

Claudius Feger, Steven E. Molis, Shaw Ling Hsu, and William J. MacKnight*

Polymer Science and Engineering Department, University of Massachusetts, Amherst, Massachusetts 01003. *Received November 9, 1983*

ABSTRACT: Model networks based on α,ω-dihydroxypoly(propylene oxides) and tris(4-isocyanatophenyl) thiophosphate were prepared. The curing kinetics were followed up to 97% conversion by measuring the change in the infrared absorption intensity of the isocyanate stretching band at 2200–2300 cm^{-1}. The overall reaction kinetics were found to be second order and are described well by a scheme consisting of competitive consecutive order reactions up to an extent of reaction of about 85% (the gel point). The observed increase in reaction rate at conversions greater than 85% is attributed to an increase in intramolecular reactions.

In the past few years dynamic mechanical tests have been widely used to monitor the changes in viscoelastic response during network formation.[1-10] The aim of such measurements is to determine the time dependence of the state of cure and the curing mechanisms of thermosets and finally to understand network formation and properties on the molecular level. Such knowledge can then lead to optimization of curing processes.

Properties of partially cured networks can be obtained by two principally different methods. The first involves quenching of the cross-link reaction by cooling or by addition of fast-reacting monofunctional agents at different reaction times to produce samples at various states of cure.[8] Disadvantages of adding monofunctional reactants are that this does not work in the postgel region of fast-curing thermosets and that the system is altered by the treatment. Some parameters, like sol content, however, can only be measured in this way.

The other method relies on measurement of properties while the cross-like reaction continues. This method requires either that the property changes caused by the ongoing cure are small in the time scale of the measurement or that they are taken into account.[6] Furthermore, to relate the measured properties to the state of cure the curing kinetics have to be known.

In this paper we describe synthesis and kinetics of a system that is well suited for investigation of properties of partially cured networks.

System

Many of the investigations of curing processes have been conducted with chemically very complex systems[1-7] so that the data obtained are difficult to explain on a molecular basis. Since the study of model networks has been successful in the interpretation of structural dependencies of fully cured networks,[11] the application of the same concept to investigate properties of partially cured networks seems reasonable.[8,10] A model network-forming system suitable for the intended studies has to fulfill the following criteria: the network formation should be noncatalytic and slow at room temperature and form no byproducts. Furthermore, there should be a convenient analytical technique to elucidate the kinetics of the curing reaction. Finally, the glass transition of the system during the cure should always be below the curing temperature. All these requirements are satisfied by a system consisting of α,ω-dihydroxypoly(propylene oxide) and tris(4-isocyanatophenyl) thiophosphate. Similar systems have been used by Andrady[12] and with a different trisisocyanate by Sung and Mark.[13]

Materials

α,ω-Dihydroxypoly(propylene oxides) of nominal molecular weight 1000 and 3000 were obtained from Aldrich Chemical Co. The molecular weights obtained by vapor pressure osmometry are 1170 and 2820. Analysis for OH groups show that the PPO's have a functionality of approximately 2.0 ± 4%. This is in agreement with the results of Sung and Mark.[13] The fraction of

0024-9297/84/2217-1830$01.50/0